University of Kent

Kent Academic Repository

Roy, Arijit, Surendra, V S, Ambresh, M, Ramachandran, R, Meka, J K, Venkatraman, V, Vijay, T, Marhas, K K, Das, A, Thirukumaran, V and others (2026) *Shock induced bottom up formation of silicon carbide (SiC) nanodust*. Monthly Notices of the Royal Astronomical Society . ISSN 0035-8711.

Downloaded from

https://kar.kent.ac.uk/117555/ The University of Kent's Academic Repository KAR

The version of record is available from

https://doi.org/10.1093/mnras/stag2104

This document version

Publisher pdf

DOI for this version

Licence for this version

CC BY (Attribution)

Additional information

Versions of research works

Versions of Record

If this version is the version of record, it is the same as the published version available on the publisher's web site. Cite as the published version.

Author Accepted Manuscripts

If this document is identified as the Author Accepted Manuscript it is the version after peer review but before type setting, copy editing or publisher branding. Cite as Surname, Initial. (Year) 'Title of article'. To be published in ***Title of Journal*** , Volume and issue numbers [peer-reviewed accepted version]. Available at: DOI or URL (Accessed: date).

Enquiries

If you have questions about this document contact ResearchSupport@kent.ac.uk. Please include the URL of the record in KAR. If you believe that your, or a third party's rights have been compromised through this document please see our Take Down policy (available from https://www.kent.ac.uk/guides/kar-the-kent-academic-repository#policies).

Shock induced bottom up formation of silicon carbide (SiC) nanodust

Arijit Roy[1,*,†], V S Surendra[1‡], M Ambresh[2], R Ramachandran[1,3], J K Meka[1], V Venkatraman[4], T Vijay[5], K K Marhas[1], A Das[3], V Thirukumaran[6], P Janardhan[1], B N Rajasekher[3] , Anil Bhardwaj[1], N J Mason[7] , B Sivaraman[1*].

[1] Physical Research Laboratory, Ahmedabad 380009, India.
[2] Indian Institute of Science, Bengaluru 560012, India.
[3] Institute of Astronomy Space and Earth Sciences, Kolkata 700054, India.
[4] Space Physics Laboratory, Vikram Sarabhai Space Centre, Thiruvananthapuram, 695022, India.
[5] Institute of Technology, Gandhinagar, 382055, India.
[6] Chikkaiah Government Arts and Science College, Erode, 638004, India
[7] The School of Physics and Astronomy, University of Kent, Canterbury CT2 7NZ, UK.

*Contact: arijit.roybwn11@gmail.com, bhala@prl.res.in

† Current address: Department of Chemistry, Indian Institute of Technology, Kharagpur, India.

‡ Current address: Department of Chemistry, Umeå University, Umeå, Sweden.

Abstract:

Silicon carbide (SiC) dust plays an important role in the interstellar molecular enrichment process by providing a finite area for surface chemistry to take place. Its robust presence in different parts of interstellar medium (ISM) and circumstellar medium (CSM) has been routinely traced by observations at the mid-infrared wavelength. It is one of the most well studied dust grains observed as a component of presolar grains in the meteorite. In this work, we experimentally investigated the bottom up formation pathway of SiC by shock processing of amorphous carbon nanodust and silicon nanopowder with a 2: 1 mass ratio (with mole fraction around 4.7:1)in the presence of hydrogen. The pre and post-shocked samples were examined using techniques including ATR-FTIR spectroscopy, XRD, and HR-TEM imaging. These results show the presence of polycrystalline (α,β) SiC and various carbon nanostructures such as carbon nanoribbons, carbon nanotubes and nanobuds. These results suggest that shock waves, especially low-velocity shock waves, in the ISM/CSM, can induce a chemical reaction between elemental C and Si, leading to the formation of polycrystalline SiC and various other forms of carbon nanostructures simultaneously.

Key words: Astrochemistry, shock waves, solid state: refractory, methods: laboratory: solid state, (ISM:) dust, extinction.

ORIGINAL UNEDITED MANUSCRIPT

Downloaded from academic.oup.com/mnras/advance-article/doi/10.1093/mnras/stag2104/9013336 by The Templeman Library user on 06 November 2026

© The Author(s) 2026. Published by Oxford University Press on behalf of Royal Astronomical Society. This is an Open Access article distributed under the terms of the Creative Commons Attribution License (https://creativecommons.org/licenses/by/4.0/), which permits unrestricted reuse, distribution, and reproduction in any medium, provided the original work is properly cited.

1. Introduction:

Silicon carbide (SiC) is one of the important components of interstellar dust (Speck *et al.* 2009). Its presence as a condensate in the outflow of carbon-rich Asymptotic Giant Branch (AGB) stars has been predicted by authors like Gilman (1969), Friedemann (1969), and McCabe (1982). Hackwell (1972), Treffers & Cohen (1974), and Goebel *et al.* (1980), were the first to ascribe the 11.2 μm infrared emission feature observed around carbon-rich AGB stars to SiC. Also, a similar absorption feature of SiC has also been observed in numerous extreme carbon stars Speck et al (Speck *et al.* 1997, Speck et al. 2009). Sub-mm observations of the stellar envelope of IRC+10216 (CW Leo) have revealed the presence of many silicon carbon-based molecules and radicals which have been attributed to the SiC radical (Cernicharo *et al.* 1989), the closed-shell ionic ring SiC_2 (Thaddeus *et al.* 1984, Cernicharo *et al.* 2010) a well-known carrier of the *Merrill and Sanford* band, rhomboidal SiC_3 (Apponi *et al.* 1999), the linear chain molecule SiC_4 (Ohishi *et al.* 1989) and in the last decade Si_2C (Cernicharo *et al.* 2015). Despite the presence of SiC as dust and many Si-C-based molecules and radicals in circumstellar envelopes, SiC dust in the diffuse ISM has not been detected. The reason behind the absence of an 11.2 μm band in the diffuse ISM is still not apparent. However, one possible explanation could be the destruction of SiC grains by O atoms. Once SiC is injected into the ISM, it can contribute to silicate dust formation (Whittet *et al.* 1990, Chen *et al.* 2022).

In presolar grains embedded in carbonaceous chondrites, SiC is the second most abundant carbonaceous grain after nano diamonds (Ott 2010). However, this abundance pattern doesn't carry forward for interstellar grains. Observation and optical constant modelling (Jones & Ysard 2022) reveals that amorphous carbonaceous and silicate dust dominates in the ISM dust compare to the nanodiamond. The presence of SiC was first detected in the Murray CM2 carbonaceous chondrites by analysing the isotopic anomalies of the noble gas trapped within them (Bernatowicz *et al.* 1987). Presolar SiC can be classified into different categories based on the isotopic proportion of the elements like C, N, Si and Al (Ott 2010). Amongst them, the most abundant grains (90%) are known as mainstream grains, and the other types are classified as A, B, X, Y, and Z (Ott 2010). In nature, SiC has been identified in 250 different polytypes. However, samples extracted from meteorites have shown only the presence of cubic (β-SiC) and hexagonal (α-SiC) phases, with β-SiC being

ORIGINAL UNEDITED MANUSCRIPT

Downloaded from academic.oup.com/mnras/advance-article/doi/10.1093/mnras/stag2104/9013336 by The Templeman Library user on 06 November 2026

the most abundant phase (Daulton *et al.* 2003, Bernatowicz et al. 1987). These grains follow a log-normal size distribution (Amari et al. 1994). In the 90s, the known grain size was limited to the range 0.3 to 3 μm (Amari et al. 1994). However, in the era of NanoSIMS, more fine-grained samples have been analysed (0.2 – 0.5 nm) and reveal that submicron to nanometre size grains are more abundant than micron size grains (Gyngard *et al.* 2010, Hoppe *et al.* 2010, Amari 2014).

SiC is thought to play a crucial role in the interstellar molecular enrichment process. Once injected into the ISM, they are exposed to harsh energetic processing, which leads to subsequent mass loss and enriches the chemical complexity in the ISM. In planetary nebulae, high-velocity outflows called fast winds generate shock waves, which process the dust by rapid heating up to several thousands of kelvin (Sevenster & Chapman 2001, Van de Steene & Van Hoof 2003). These nebular shocks also contain ions, which bombard dust grains and implant themselves on their surface (Heck *et al.* 2009).

Like other carbonaceous dust the formation pathway of SiC dust in circumstellar conditions is still an evolving topic (Speck et al. 2009). Shock processing of dust precursors could lead to the formation of dust in astrophysical sources, such as in Nova V2891 Cyg (Kumar *et al.* 2022). Laboratory experiments simulating stellar shock heating (up to 1300 K) followed by ion bombardment (150 keV Xe) on SiC grains showed the formation of carbon nanostructures, including fullerenes and graphite (Bernal *et al.* 2019). The thermal decomposition of SiC has also been found to produce carbon nanostructures, such as hemispherical fullerenes and Carbon Nanotube (CNT) (Kusunoki *et al.* 1997, Watanabe *et al.* 2001, Bernal *et al.* 2022). Experiments have also shown that exposure of graphitised SiC to atomic H, under simulated interstellar conditions, leads to the formation of Polycyclic Aromatic Hydrocarbon (PAH) molecules (Merino *et al.* 2014). Thus it is likely that SiC works as a catalyst in interstellar chemistry.

A high-intensity shock tube can be used to simulate the low velocity circumstellar shock conditions in the laboratory. In recent years, there has been a growing interest in shock tubes in the field of high-temperature astrochemistry (Biennier *et al.* 2017, Roy *et al.* 2022b, Roy *et al.* 2022a, Chakraborty *et al.* 2024, Roy *et al.* 2025, Singh *et al.* 2025) and astrobiology (Singh *et al.* 2020, Dhage *et al.* 2025). A recent review by (Roy *et al.* 2023) summaries various results obtained using shock tubes in the area of laboratory

ORIGINAL UNEDITED MANUSCRIPT

Downloaded from academic.oup.com/mnras/advance-article/doi/10.1093/mnras/stag2104/9013336 by The Templeman Library user on 06 November 2026

astrochemistry by different research groups. In the present work a high-intensity shock tube was used to simulate the low velocity circumstellar shock conditions in the laboratory. We processed a mixture of amorphous carbon and silicon nanopowder (2:1 mass ratio) in the presence of molecular hydrogen gas (H_2) using a high-intensity shock with a Mach number ~ 5.3, producing a reflected shock temperature ~ 3900 K for 2 ms. Amorphous carbon was chosen in this experiment since carbonaceous dust in different astrophysical regions is predominately amorphous rather than graphitic (Sorrell 1990). The presence of H_2 is important since it is the most abundant molecule observed in the different parts of ISM and can play a key role in the nucleation process of dust grains (Cherchneff 2000). The shock-processed samples were analysed using Attenuated Total Reflectance-Fourier Transform Infrared Spectroscopy (ATR-FTIR), X-ray diffraction (XRD), High-Resolution Transmission Electron Microscopy (HR-TEM), and Energy Dispersive X-ray (EDX) mapping and spectroscopy.

2. Experimental Methodology:

The presented experiments were carried out using the High Intensity Shock Tube for Astrochemistry (HISTA) housed at the Physical Research Laboratory, India. HISTA is a 7 m long shock tube with 2 m driver section and 5 m driven section. A detailed description of HISTA, its operational procedures, capabilities and the methods to measure the shock pressure, reflected shock pressure and temperature can be found in the work by Roy et al (Roy et al. 2022a, Roy et al. 2022b, Roy et al. 2025). About 0.1 gm of powder sample consisting of a 2:1 mass ratio mixture of carbon nanopowder particle size <100 nm; Sigma-Aldrich) and silicon nanopowder particle size <100 nm; Sigma-Aldrich) was prepared. The mole fraction for the carbon is 0.824 and for the Si is 0.176. Therefore, C:Si is around 4.7 :1. This chosen carbon-to-silicon ratio in this experiment does not exactly reproduce the circumstellar abundance; it mimics the carbon-rich environment of C stars, where SiC condensation occurs. In the circumstellar shell, Si is usually locked up into gas-phase Si-bearing molecules such as SiC_2, SiC, Si_2C, SiS, and SiO, with SiC_2 serving as a precursor of SiC. Si is relatively less abundant in the circumstellar shell compared to our sample, but the excess Si has been chosen to ensure the formation of a detectable amount of SiC under shock-heating conditions on a millisecond timescale. This laboratory enrichment is necessary because, in the circumstellar

ORIGINAL UNEDITED MANUSCRIPT

Downloaded from academic.oup.com/mnras/advance-article/doi/10.1093/mnras/stag2104/9013336 by The Templeman Library user on 06 November 2026

shell, the formation and build-up of detectable amount of SiC takes place over a much longer astrophysical time scale, whereas the experiment has been designed to mimic such a formation scenario in a short time scale (ms). Helium (He) was used as a driver gas and in the driven section we used a 0.15 bar mixtures of Ar and H_2 with 80: 20 mole fraction ratios. The mole fraction for H is 0.40. Therefore, the reacting environment is qualitatively represented by a Si:C:H abundance ratio of approximately 1:4.7:0.4. Because the gas mixture is reactive therefore, Rankin-Hugoniot jump equations can't accurately estimate the reflected shock temperature and pressure accurately. Therefore, in this work we used NASA's CEARUN [1] shock tube module to estimate the reflected shock temperature and pressure. This module[1] self-consistently estimates the post-shock temperature and pressure by solving the mass, momentum, and energy conservation equations across the shock front, together with chemical kinetics calculations based on the minimisation of Gibbs free energy. This code uses initial gas mixture ratios, experimentally measured shock velocity and initial gas temperature and pressure (driven section) as inputs to compute the reflected shock temperature and pressure. The shock velocity was measured from the shock pressure response curve as shown in supplementary **Fig S1**. Using the shock velocity (which is ~ 1.8 km s^{-1} or Mach 5.1 in this work), and the mole fraction of the driven gas mixtures in the CEARUN shock module we estimate the reflected shock temperature ~ 3900 K. The shock processing time scale persists about 2 ms, during which the sample is processed at a uniform gas temperature (3900 K) and pressure (29 bar). Details of different experimental parameters associated with this experiment is tabulated in **Table1**. After the shock processing the shocked gas in the tube returned to an equilibrium pressure ~ 18 bar. We then evacuate this high pressure gas using a leak valve and collect the processed sample from the shock tube. These processed samples were further analysed with the help of ATR FTIR spectroscopy, XRD, HR-TEM, EDX techniques.

[1] https://cearun.grc.nasa.gov

ORIGINAL UNEDITED MANUSCRIPT

Downloaded from academic.oup.com/mnras/advance-article/doi/10.1093/mnras/stag2104/9013336 by The Templeman Library user on 06 November 2026

Table 1: Experimental parameters associated with this experiment

Parameter	Initial Gas	Incident Shocked Gas	Reflected Shocked Gas
Shock velocity (m s^{-1})	1800	—	—
Pressure (bar)	0.15 (driven section)	4.90	26.20
Temperature (K)	300	2408	3871
Ar mass fraction	0.9875	0.9875	0.9875
H mass fraction	—	1.04×10^{-4}	3.07×10^{-3}
H_2 mass fraction	—	1.24×10^{-2}	9.39×10^{-3}

3. Results:

3.1 ATR-FTIR Spectroscopy:

ATR – FTIR Spectra of the pre and post-shocked sample over the wavelength range between 7 to 20 μm are shown in **Fig 1**. The spectra were acquired using a Nicolet iS50 FTIR spectrometer with a resolution of 2 cm^{-1} with total data acquisition time ~ 1 minutes 32 seconds. The spectra of the unshocked sample, marked by black colour in **Fig 1(a)**, have a broad plateau-like feature spanning between 8.2 and 10.3 μm. This band is assigned to the Si-O-Si asymmetric stretching motion (Ellerbrock *et al.* 2022), where O is an impurity, as silicon has good surface activity.

The IR spectra of the shocked sample shown in **Fig 1 (b-c)** were taken from two parts of the same sample. These two spectra are almost identical and have two very distinct IR features. One occurs between 8.2 to 10.3 μm, which is also present in the unshocked sample due to surface reaction between Si and atmospheric O. The other feature exhibits a sharp asymmetric Gaussian profile, peaking around 12.6 μm (~ 790 cm^{-1}). This peak represents silicon carbide's fundamental resonance absorbance feature in the IR (Spitzer *et al.* 1959, Hofmeister *et al.* 2009). The phonon modes of SiC, usually observed at 11.3 μm in carbon stars, show variability due to various factors, with particle size and crystal type being the most significant (Mutschke *et al.* 1999). The infrared spectrum of the post-shock samples shows SiC at 12.6 μm, possibly due to the longitudinal optical phonon mode in the SiC lattice. From the resonance absorbance band, it is difficult to define about the structure of the synthesized silicon carbide as both hexagonal and cubic

ORIGINAL UNEDITED MANUSCRIPT

Downloaded from academic.oup.com/mnras/advance-article/doi/10.1093/mnras/stag2104/9013336 by The Templeman Library user on 06 November 2026

phases have similar IR features (Spitzer et al. 1959). The gradual rise of the baseline in both shocked and unshocked IR spectra could be due to the high absorption of the IR beam by carbonaceous dust analogues (Pino et al. 2008). Carbonaceous particles show absorption throughout the IR range, and for the ATR-FTIR configuration, the penetration depth increases with the IR wavelength, and therefore, the absorption increases with the increasing IR wavelength. This leads to the rise in the baseline in the IR spectra of the both shocked and unshocked samples.

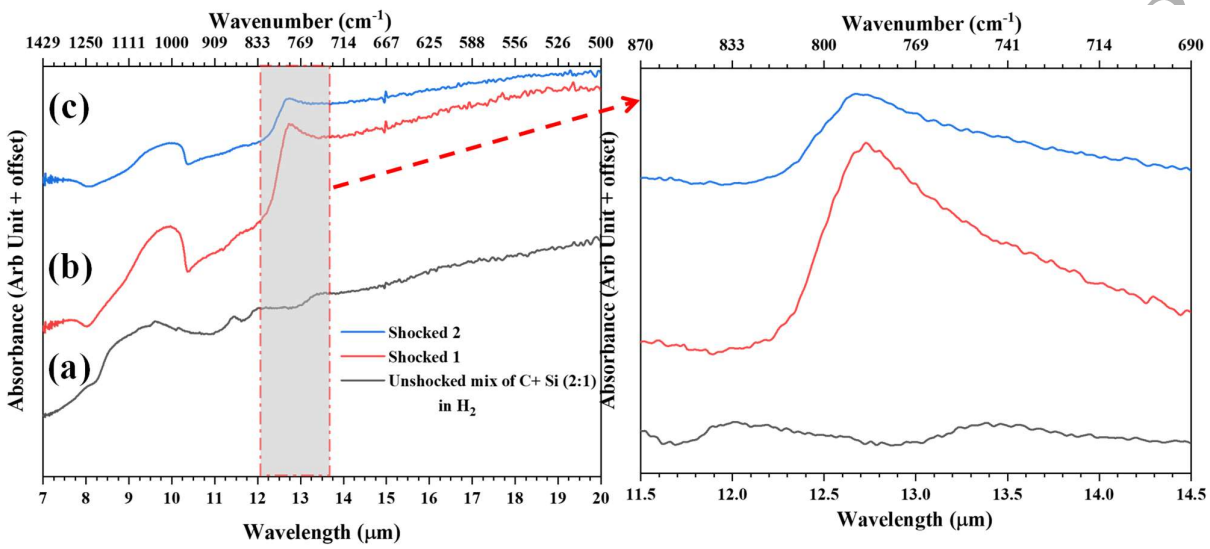


Fig 1: *ATR FTIR Spectra of both the pre and post-shocked sample. The right hand panel, indicated by a red arrow, shows an enlarged view of the shaded 12 to 14 μm region in the left hand panel, which contains the IR-active mode of SiC. The unshocked sample remains featureless in this spectral window.*

3.2 XRD analysis:

XRD patterns of both pre and post-shocked mixtures of C plus Si (2:1) are shown in **Fig. 2**. These patterns are normalised to the same scale before plotting, and offset is applied for visual clarity. Bragg's equation has been employed to calculate the interplanar spacing (d) of different XRD peaks. **Fig. 2(a)** represent the XRD patterns of the unshocked sample. The broad feature around 26º, marked by a black star, shows amorphous carbon. The other peaks, marked by orange stars, are the well-known diffraction pattern of silicon from the

ORIGINAL UNEDITED MANUSCRIPT

Downloaded from academic.oup.com/mnras/advance-article/doi/10.1093/mnras/stag2104/9013336 by The Templeman Library user on 06 November 2026

standard XRD database (CODID: 1526655).

Fig 2 (b) shows the XRD patterns of the shocked sample. It has many new peaks compared to its unshocked counterpart. Some new peaks are marked by a purple cube and a blue hexagon, and some by a blue triangle. We can also see the presence of both silicon and amorphous carbon in the shocked sample, with an orange star and a black star marking their corresponding peaks respectively. Those peaks marked by a blue triangle show the presence of Al, which originate due to the rupture of the Al diaphragm used in HISTA. The peaks marked by a purple cube are around 35.86º,41.62º, 60.20º, and 72º. We compared these peak positions with the synthetic XRD pattern of cubic SiC (β) shown in **Fig 2 (c)** and found a good match. This synthetic XRD pattern of cubic SiC (β) was generated using VESTA (Izumi & Momma 2007), and its unit cell information was taken from CODID:1011031. A less intense peak around 33.86º, marked by a blue hexagon is assigned to the hexagonal SiC phase. One can find the details of the crystallographic information of the shocked sample, such as Miller indices, interplanar d spacing and comparison of d spacing with the standard data in **Table 2**. We also noticed that the band peaking 26 º in **Fig 2 (b)** gets sharper compared to the band present at around 26 º in **Fig 2 (a)**. This suggests shock- induced graphitisation of the amorphous carbon.

ORIGINAL UNEDITED MANUSCRIPT

Downloaded from academic.oup.com/mnras/advance-article/doi/10.1093/mnras/stag2104/9013336 by The Templeman Library user on 06 November 2026

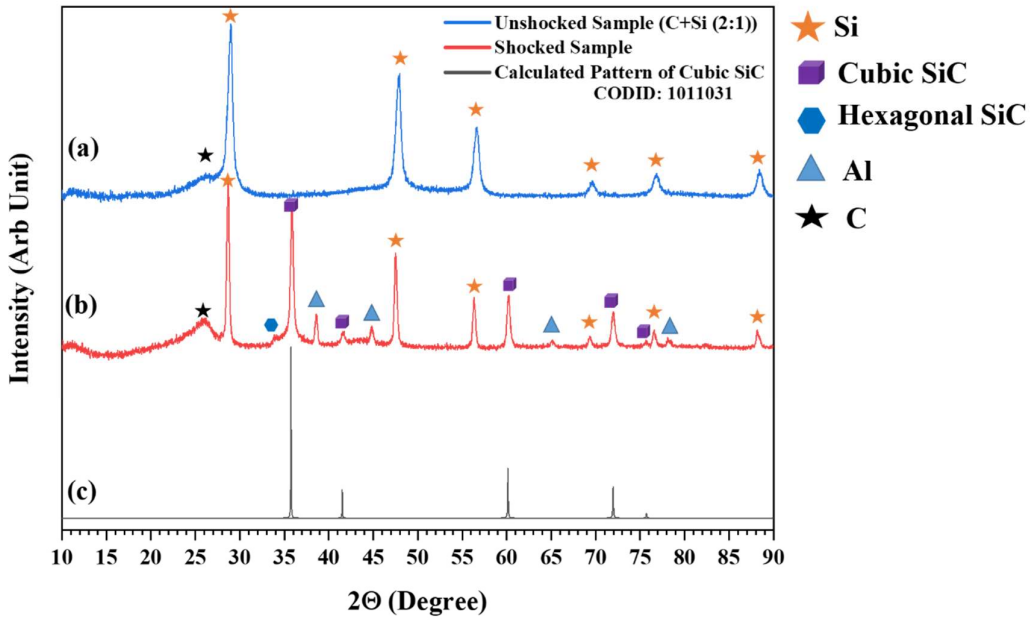


Fig 2: *(a) XRD Pattern of the unshocked sample, (b) XRD pattern of the shocked sample, and (c) synthetic XRD pattern of cubic SiC (β).*

Thus, the XRD results clearly shows that shock processing of the mixtures of amorphous C and Si (2:1 mass ratio) in the presence of H_2 gives rise to crystalline silicon carbide with both cubic and hexagonal phases present. The cubic phase is found to be more dominant. We also see possible indications of shock-induced graphitisation. It should be noted that the Si peaks in the shocked sample are sharper compared to the unshocked sample. This observation indicates an increase in the crystallite size of Si induced by shock processing ultimately leads to crystal growth in the shocked sample.

ORIGINAL UNEDITED MANU

Downloaded from academic.oup.com/mnras/advance-article/doi/10.1093/mnras/stag2104/9013336 by The Templeman Library user on 06 November 2026

Table 2: *XRD peaks observed in the shocked sample along with their corresponding -spacing values and their assignments to different crystalline phases (β-SiC, Hexagonal SiC, C, and Si).*

		Assignment (Miller indices (d -spacing in Å))				
2θ (°)	**θ (°)**	**d (Å) (Experimental)**	**β- SiC CODID:1011 031**	**Hexagonal SiC**	**Carbon**	**Si CODID: 1526655**
26.06	13.03	3.42			**2 0 0 (3.42)**	
28.66	14.33	3.11				**1 1 1 (3.11)**
33.83	16.92	2.65		**1 0 1 (2.65)**		
35.86	17.93	2.5	**1 1 1 (2.51)**			
41.62	20.81	2.17	**2 0 0 (2.17)**			
47.52	23.76	1.91				**2 2 0 (1.90)**
56.33	28.17	1.63				**3 1 1 (1.62)**
60.2	30.1	1.54	**2 2 0 (1.53)**			
69.36	34.68	1.35	**4 0 0 (1.34)**			
71.99	36	1.31	**3 1 1 (1.31)**			
75.74	37.87	1.25	**2 2 2 (1.25)**			
76.58	38.29	1.24				**3 3 1 (1.23)**
78.17	39.09	1.22				
88.18	44.09	1.11				**4 2 2 (1.09)**

3.3 HR-TEM imaging and elemental mapping:

HR-TEM analysis of the shock-processed samples was carried out using a Titan Themis 300 S/TEM from Thermo. The samples were ultrasonicated in ethyl alcohol for 15 minutes, then drop-cast on a Quantifoil grid and allowed to dry in a chemically inert atmosphere overnight. Before the imaging analysis started, these drop cast grids were plasma cleaned using Ar-O_2 plasma to reduce any chance of further contamination. Throughout the investigation, the HR-TEM was operated at 300 keV. The lattice spacing of the crystalline structures observed in this work were calculated using the ImageJ (Abràmoff *et al.* 2004) software.

HR-TEM images of the shocked samples are presented in **Fig. 3(a-g)**. The low magnification image in **Fig. 3(a)** (a 200 nm scale size) shows sheets-like carbon nanostructures. At a higher magnification

ORIGINAL UNEDITED MANUSCRIPT

Downloaded from academic.oup.com/mnras/advance-article/doi/10.1093/mnras/stag2104/9013336 by The Templeman Library user on 06 November 2026

(Fig. 3(b)) numerous solid condensates were observed with particle size ranges between 17 to 90 nm.

Fig. 3(c) shows the coexistence of two distinct crystalline phases. The reciprocal lattice orientation of the region with in the red box shows in Inset 1 indicates an interplanar d spacing around 0.25 nm, and it is assigned to the (1 1 1) plane of β-SiC (CODID:1011031). The area within the yellow box has its reciprocal orientation in Inset 2, which shows interplanar d spacing is around 0.34 nm, corresponding to graphite's (002) plane (Li *et al.* 2007).

Fig 3 (d) indicates the presence of many randomly oriented elongated particles, a few of these structures can be recognised as multiwall carbon nanotubes (MWCNT) marked by a red arrow. An enlarged view of such an MWCNT with an internal diameter of about 5 nm, within the yellow box, is shown in the inset. **Fig. 3 (e)** shows the presence of a MWCNT, from another parts of the same sample with an inner diameter of approximately 5 nm marked by a red arrow. A hemispherical structure found to be attached at its end marked by a yellow arrow. The inset shows a close view of the hemispherical object, with a diameter of around 0.7 nm. This type of structure is usually called a carbon nanobud, where a fullerene is attached to the outer wall of a carbon nanotube (Duan *et al*. 2017, Bernal *et al*. 2017, Roy *et al*. 2022).

Fig. 3(f) shows the presence of a crystalline domain, and the inset indicates the reciprocal lattice orientation of area with in red box. The interplanar d spacing was found to be around 0.25 nm, which corresponds to the (111) plane of β-SiC (CODID:1011031).

Fig. 3(g) shows the presence of three distinct crystalline domains marked by a blue box, a red box, and a yellow box. Their corresponding reciprocal lattice patterns in insets 1- 3 reveals interplanar d-spacing of ~ 0.25 nm, 0.31 nm, and 0.27 nm, corresponding to the (1 1 1) plane of β-SiC (CODID:1011031), the (1 1 1) plane of Si (CODID: 1526655), and the hexagonal SiC.

Fig. 4(a) shows the High-Angle Annular Dark Field (HAADF) image of the shocked sample. The HAADF technique is sensitive to the atomic number (Z) of the elements present in the sample, with brighter areas indicating regions containing higher Z-value elements compared to the relatively less bright areas. This suggests that the brighter spots in **Fig. 4(a)** are composed of Si, while the less bright areas contain C. This is further confirmed by the individual elemental mapping of C in **Fig. 4(b)** and Si

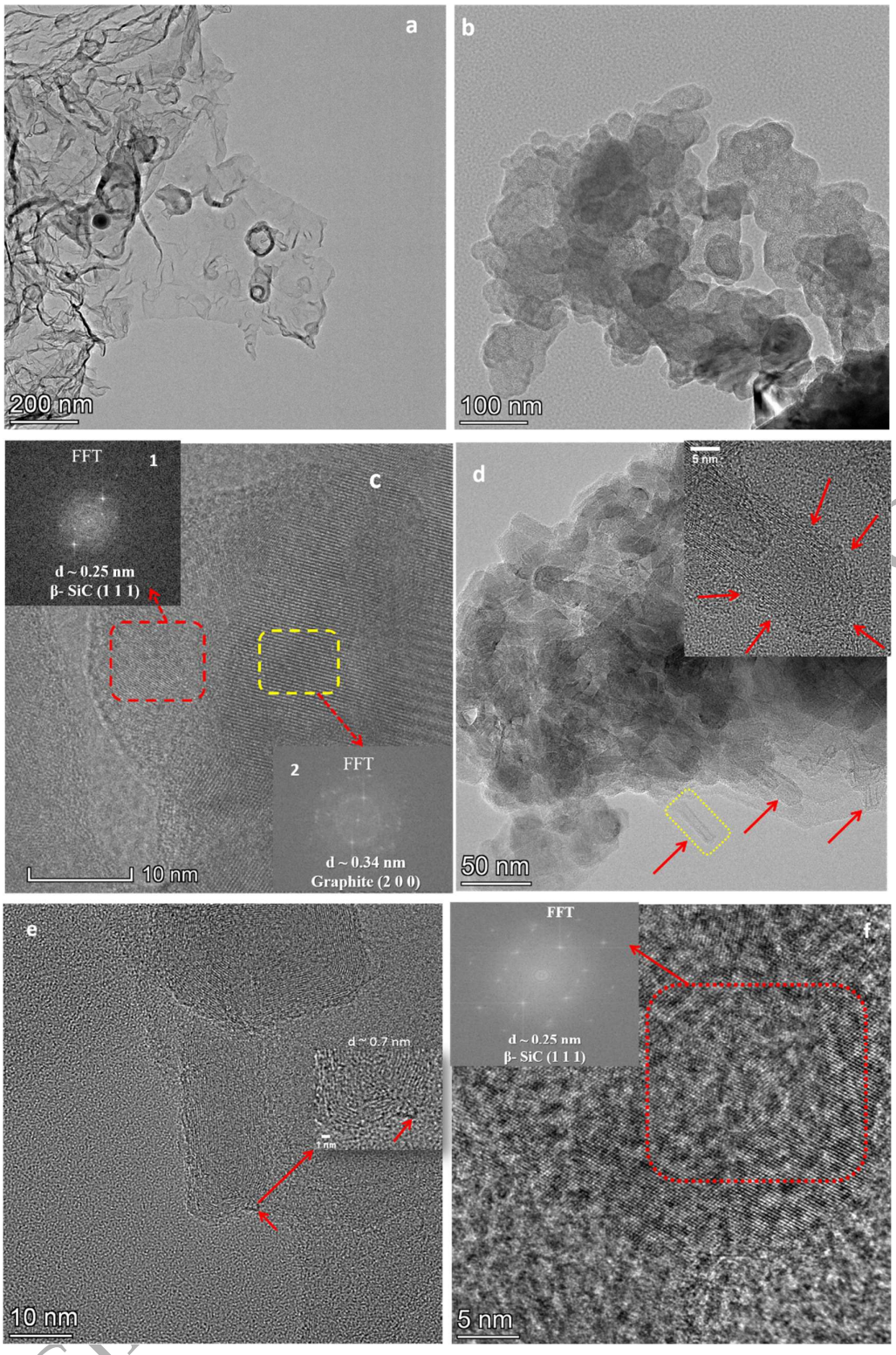
ORIGINAL UNEDITED MANUSCRIPT

Downloaded from academic.oup.com/mnras/advance-article/doi/10.1093/mnras/stag2104/9013336 by The Templeman Library user on 06 November 2026

in **Fig. 4(c)**. To estimate the Si:C ratio in the shocked sample we carried out EDX analysis. EDX spectra of the shocked sample is shown in **Fig. 4(d)**. EDX analysis of the shock-processed sample revealed the presence of C and Si with atomic concentrations of 85.21 % and 14.79 %, respectively, corresponding to an atomic C:Si ratio of approximately 5.8:1. The carbon-rich composition is consistent with the initial excess carbon in the precursor mixture and indicates that only a fraction of the available silicon participated in SiC formation. We also observed the presence of oxygen (O), aluminium (Al), and copper (Cu) in the EDX spectra. The aluminium detected is likely due to the rupture of the aluminium diaphragm, while the oxygen is a result of the oxidation of residual silicon in the shocked sample. The copper signature is attributed to the copper TEM grid.

ORIGINAL UNEDITED MANUSCRIPT

Downloaded from academic.oup.com/mnras/advance-article/doi/10.1093/mnras/stag2104/9013336 by The Templeman Library user on 06 November 2026



ORIGINAL MANUSCRIPT

Downloaded from academic.oup.com/mnras/advance-article/doi/10.1093/mnras/stag2104/9013336 by The Templeman Library user on 06 November 2026

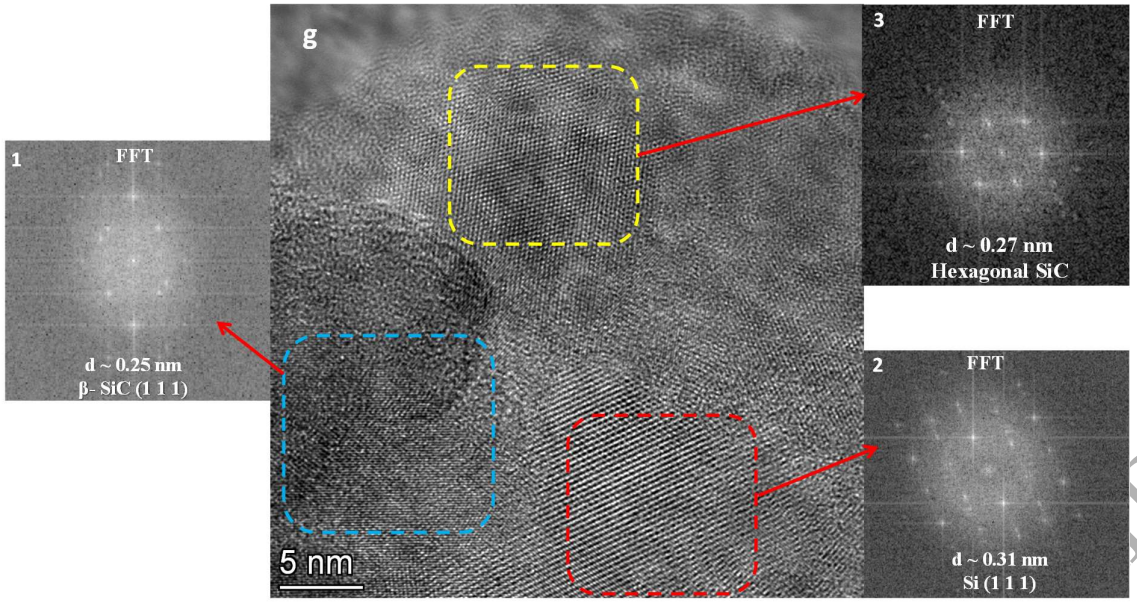
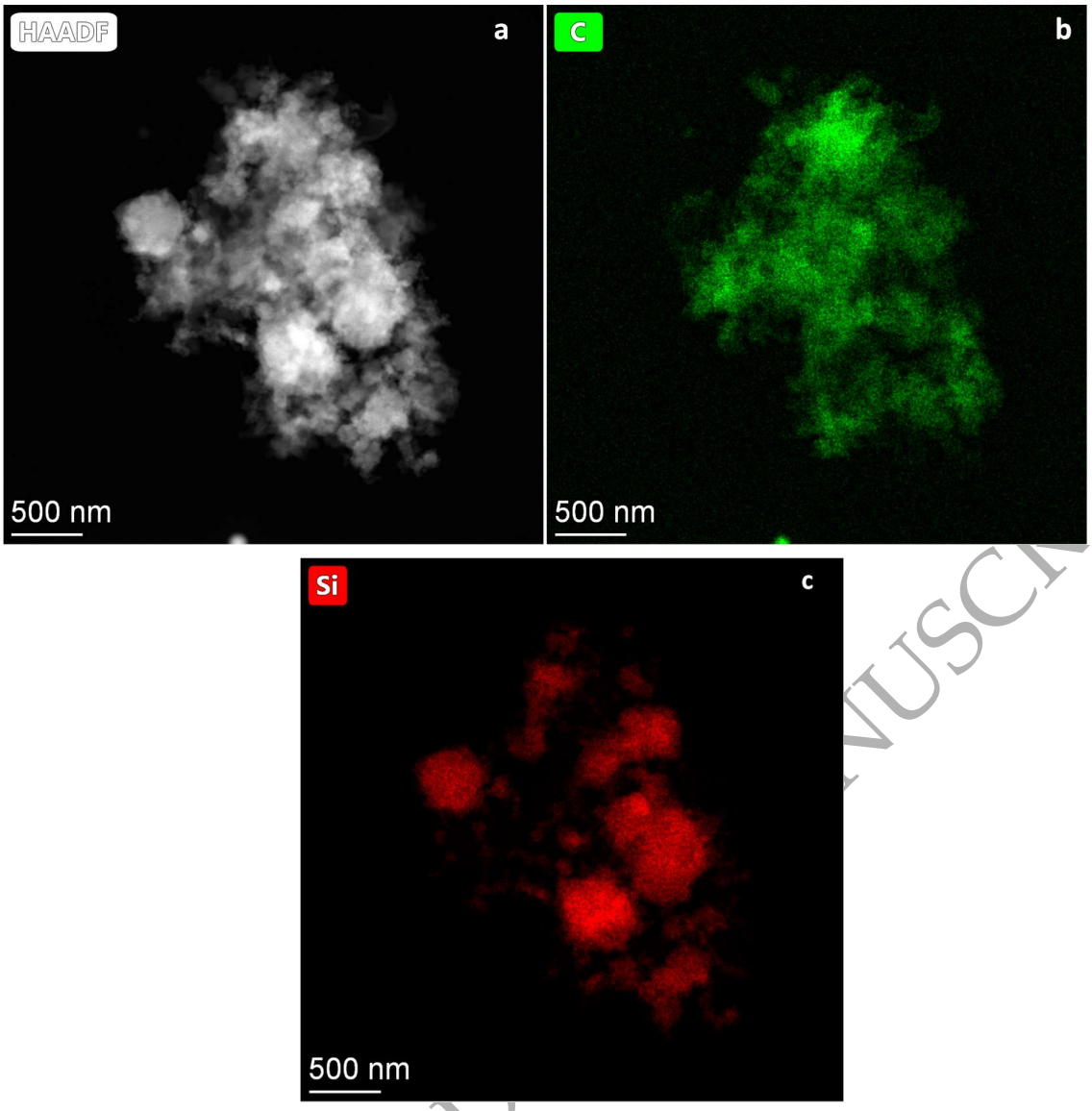


Fig 3 *HR-TEM images of the shock-processed sample. Panels (a) and (b) show sheet-like carbon nanostructures at different magnifications. Panel (c) shows the coexistence of cubic SiC and graphitic carbon. Panel (d) shows a multi-walled carbon nanotube (MWCNT), while panel (e) shows a carbon nanobud. Panel (f) displays the (111) lattice planes of crystalline β-SiC. Panel (g) shows lattice fringes corresponding to crystalline SiC and Si phases.*

ORIGINAL UNEDITED MANUSCRIPT

Downloaded from academic.oup.com/mnras/advance-article/doi/10.1093/mnras/stag2104/9013336 by The Templeman Library user on 06 November 2026



ORIGINAL UNED MANUSCRIPT

Downloaded from academic.oup.com/mnras/advance-article/doi/10.1093/mnras/stag2104/9013336 by The Templeman Library user on 06 November 2026

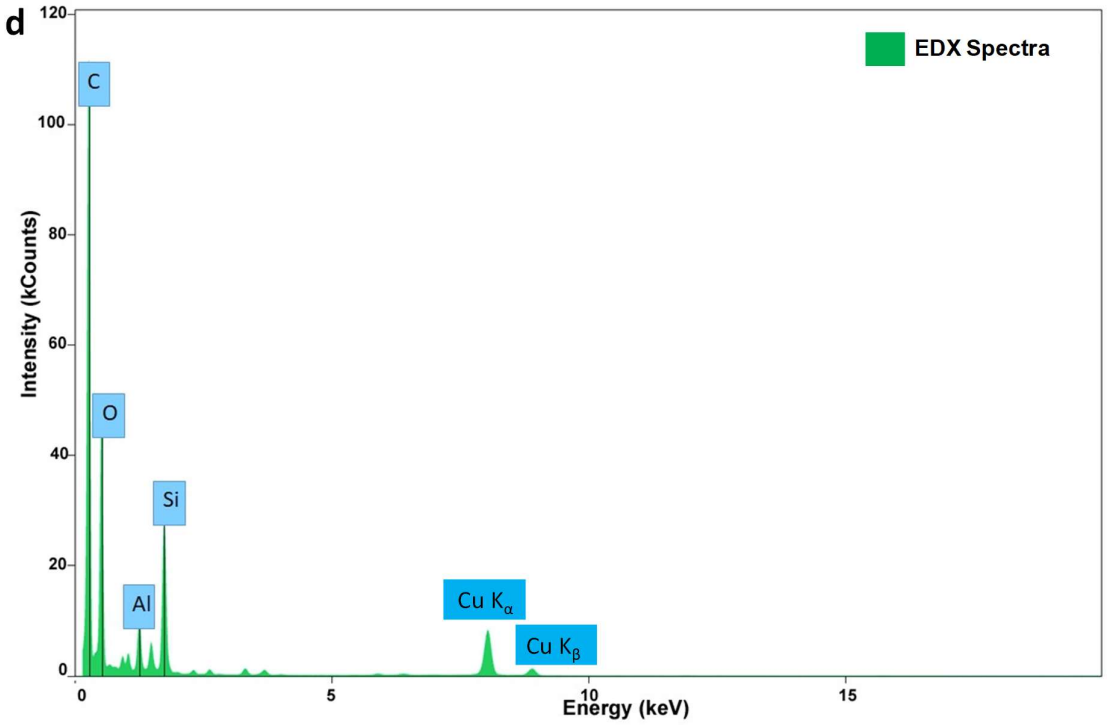


Fig4*: HAADF-STEM and EDX analyses of the shock-processed sample: (a) HAADF-STEM image; (b, c) EDX elemental maps showing the distribution of carbon (C) and silicon (Si), respectively; and (d) EDX spectrum confirming the elemental composition of the sample.*

4. Discussions:

The presented results reveal that we have synthesised SiC and various carbon nanostructures by subjecting mixtures of amorphous carbon nanopowder and Si nanopowder in a proportion of a 2:1mass ratio and 4.7:1 mole fraction ratio in the presence of H_2 to an extreme shock wave with Mach number 5.1 and estimated reflected shock temperature ~ 3900 K. Cubic SiC is found to be the dominant component compared to hexagonal SiC. Apart from the SiC, we also see the presence of various carbon nanostructures such as carbon nanosheets, nanoribbons, carbon nanotubes, nanobuds, and graphite. SiC has robust applications in semiconductor industries and different methods have been tried to synthesise SiC grains, such as chemical vapour deposition (CVD) methods (Huisken *et al.* 1999). Where the SiC grains formed due to the strong CO_2 laser-induced decomposition of the mixtures of SiH_4 and C_2H_2 (Huisken et al. 1999). Shock tubes have been used to

ORIGINAL UNEDITED MANUSCRIPT

Downloaded from academic.oup.com/mnras/advance-article/doi/10.1093/mnras/stag2104/9013336 by The Templeman Library user on 06 November 2026

synthesise SiC from gaseous precursors, such as the mixtures of SiH_4 and CH_4 in the temperature range from 800 – 3600 K, and the pressure range 0.46 to 4.16 atm (Carmer & Frenklach 1989). Similarly, Frenklach et al (Frenklach *et al.* 1989) showed the formation of SiC grains by shock processing of the gaseous mixtures of SiH_4, CH_4 and almost 60% of H_2. They explored the temperature range between 1200 and 2000 K and the pressure between 1.07 and 1.56 atm. These experiments can be considered as a top-down pathway of SiC dust formation where shock-induced destruction of SiH_4 provides Si and CH_4 as a source of C. In contrast, in this work, we have explored the bottom-up formation route of SiC starting from the elements C and Si. Also, we have studied a high-temperature formation route ~3900 K for 2 ms, mimicking low-velocity circumstellar shock processing of cosmic carbonaceous dust analogue.

By combining the results from the IR spectroscopy, XRD, and HR-TEM analysis, and considering the thermodynamic parameters such as reflected shock temperature (T_5) and reflected shock pressure (P_5), we have tried to formulate a possible formation pathway of SiC and other carbon nanostructures in this experiment. At T_5 ~ 3900 K, shock-heated Ar atoms collide with the H_2 present in the driven gas and can lead to the dissociation of H_2 (Patch 1962) via the following reaction:

$$H_2 + Ar \rightarrow 2H + Ar \qquad (1)$$

From the CEARUN shock code output in **Table 1** we observed presence of the atomic hydrogen in the both in the incident and the reflected shock conditions along with molecular hydrogen. During the incident shock condition, at a shock temperature 2400 K and pressure around 4.8 bar, the mass fraction of atomic hydrogen is estimated ~ 1.04×10^{-4}, and for molecular hydrogen it is ~ 1.24×10^{-2}. This indicates a partial thermal dissociation of molecular hydrogen during the incident shock heating. Whereas for the reflected shock condition at a temperature ~ 3800 K and pressure ~ 26.2 bar, the estimated mass fraction of atomic hydrogen is about 3.1×10^{-3}, for the molecular hydrogen it is about 9.39×10^{-3}. This suggest an increment of H_2 dissociation rate with the increase of shocked gas temperature. But due to the high pressure for the both incident and reflected shock conditions the recombination from atomic to molecular hydrogen has also been taken place in parallel to the dissociation and therefore molecular hydrogen has only partially dissociated.

ORIGINAL UNEDITED MANUSCRIPT

Downloaded from academic.oup.com/mnras/advance-article/doi/10.1093/mnras/stag2104/9013336 by The Templeman Library user on 06 November 2026

C and Si will also be heated due to the collision with shock-heated Ar atoms via eq (2) and (3).

$C + Ar \rightarrow C^{*} + Ar$ (2)

$Si + Ar \rightarrow Si^{*} + Ar$ (3)

The '*' denotes the thermally excited state of C and Si. According to the corresponding phase diagram, C (Bundy 1989) will be in the vapour phase at a gas temperature of ~ 3900 K and pressure of ~ 25 bar, whereas Si (Bundy 1964) will also melt at this high temperature and pressure. However, the phase diagram describes equilibrium states and does not provide the timescale required for phase transition. Sublimation kinetics under shock heating are typically monitored using optical emission spectroscopy and laser interferometry (Biennier et al. 2017, Chakraborty et al. 2024, Willhardt *et al.* 2024). The present HISTA setup does not include *in-situ* optical emission spectroscopy, so our interpretation is based on the analysis of the recovered shock-processed dust. In our shock tube experiment, the heating duration is only about 2 ms; therefore, carbon and silicon nanoparticles (< 100 nm) could be sublimated and turned in to a supersaturated vapour containing Si, C, and H species, thereby initiating non-equilibrium chemical reactions.

The thermally excited carbon C* can react with another excited C atom to make C_2, and this reaction will continue towards forming of n numbers of larger carbon clusters (C_n) as described in eq (4).

$C + C + Ar \rightarrow C_2 + Ar \rightarrow \text{------} \rightarrow n\,C_n$ (4)

At high temperatures, C_2 can react with molecular hydrogen and produce C_2H via eq (5). Although a significant amount of H_2 will dissociate at a high temperature, recombination has also taken place via a third body/ surface reaction as suggested by CEARUN output documented in **Table 1**.

$C_2 + H_2 \rightarrow C_2H + H$ (5)

The Eq (5) is a high enthalpy reaction (~ 100 kJ mol^{-1}) and only possible above the temperature of ~ 550 K (Pitts *et al.* 1982). Hence, eq (5) is likely to occur in our experimental conditions. C_2H can further react with H_2 and form acetylene (C_2H_2). C_2H can react with atomic carbon and form C_3 (Santoro *et al.* 2020), which can again contribute to the formation of larger carbon clusters. At the high-temperatures the formation of sp^2 bonds are energetically favourable (Derjaguin *et al.* 1977). Therefore, we see most of the observed structures in the TEM images (**Fig 3 (c-e))** of the shocked samples are either graphitic such as carbon nanoribbons, MWCNT or polycrystalline graphite. The possible reactions hence can be written as

ORIGINAL UNEDITED MANUSCRIPT

Downloaded from academic.oup.com/mnras/advance-article/doi/10.1093/mnras/stag2104/9013336 by The Templeman Library user on 06 November 2026

$C_2H + H_2 \rightarrow C_2H_2 + H$ (6)

$C_2H + C \rightarrow C_3 + H_2$ (7)

Acetylene can again react with the C, form C_3, and release molecular hydrogen. It can also react with shock-heated Si atoms and produce SiC_2H (MacKay & Charnley 1999). The following reactions can be written as

$C_2H_2 + C \rightarrow C_3 + H_2$ (8)

$C_2H_2 + Si \rightarrow SiC_2H + H$ (9)

The SiC_2H can further react with C to form SiC_3 (MacKay & Charnley 1999) via the following reaction:

$SiC_2H + C \rightarrow SiC_3 + H$ (10)

SiC_3 can contribute to the formation of larger $(SiC)_n$ clusters. In the gas phase, both Si and C can react and SiC forms.

$C + Si \rightarrow SiC$ (11)

The rapid quenching at approximately 10^6 K s^{-1}, triggered by the arrival of the expansion wave, froze the reacting Si–C system before it could anneal into a lower-energy crystalline configuration.

The XRD (in **Fig. 2(a))** and the HRTEM images (in **Fig. 3(c, f, g)**) of the shocked samples suggest a preponderance of cubic SiC over the hexagonal SiC in shocked sample. The condensation of SiC from a supersaturated vapour is well known to favour the formation of the cubic (3C) polytype (Knippenberg 1963). According to (Heine *et al.* 1991), rapid growth under non-equilibrium conditions favours the formation of cubic SiC because the atoms do not have enough time to rearrange into hexagonal structures. This kinetic interpretation is supported by thermodynamic studies. First-principles calculations by (Scalise *et al.* 2019) showed that 3C-SiC is the thermodynamically stable polytype below approximately 1750–2400 K, a temperature range that the system likely come across during rapid cooling and nucleation. Furthermore, using classical two-dimensional nucleation theory, (Kakimoto & Nakano 2025) demonstrated that 3C-SiC becomes thermodynamically more favourable than 4H-SiC under conditions of high carbon super saturation, which is consistent with the present experimental conditions.

Experimental evidence also supports this interpretation. (Langenderfer *et al.* 2022) reported the formation of predominantly cubic SiC during detonation-driven blast-wave compression of Si–C mixtures at approximately 3300 K followed by rapid quenching. Although the pressure employed in our study (~29 bar or 2900 kPa) is significantly lower than that in their experiments (27 GPa), the peak temperatures are comparable, and both studies involve rapid cooling from a highly

ORIGINAL UNEDITED MANUSCRIPT

Downloaded from academic.oup.com/mnras/advance-article/doi/10.1093/mnras/stag2104/9013336 by The Templeman Library user on 06 November 2026

supersaturated state. Therefore, our results suggest that shock-induced flash heating followed by rapid quenching provides an effective pathway for the preferential formation of cubic SiC under non-equilibrium conditions.

There are also possibilities of forming various gas phase hydrocarbon and organosilicon molecules by the reactions amongst the excited C, Si and H_2 (Accolla *et al.* 2021, Martínez *et al.* 2020, Santoro et al. 2020). However, in this present study, we have not analysed the gas phase products. Hence no separate discussion has been carried out on the gas phase molecules in the shocked gas.

The XRD and the TEM analysis of the shocked samples showed simultaneous formation of graphitised carbonaceous dust together with the other sp^2 bonded carbon nanostructures such as MWCNT, and carbon nanobuds along with SiC. There exist various ways to graphitise the amorphous carbon, which include (1) catalytic active transition metals, (2) laser irradiation, (3) ion irradiation, (4) mechanical shear forces, and (5) high-temperature annealing with high-pressure (Loh & Baillargeat 2013), and (6) shock processing (Roy et al. 2022b). The shock processing of amorphous carbon nanodust around 7300 K for 2 ms in the hydrogen reduced conditions showed the formation of various carbon nanostructures such as carbon onions, graphene, nanobud, MWCNT etc (Roy et al. 2022b). In this work, the incorporation of hydrogen in the shock process plays a crucial role in transforming amorphous carbon into these diverse carbon nanostructures at a low shock-heated gas temperature ~ 3900 K, compared to the work by Roy et al (Roy et al. 2022b). The atomic hydrogen produced because of the shock heating (equation1) is much more reactive than the molecular hydrogen, and acts as a catalyst reducing the graphitisation barrier during the transformation of amorphous carbon into graphite by promoting the formation of sp^2 bond (Wang *et al.* 1995). The graphitisation process involves rearranging carbon atoms into a highly ordered, layered structure characteristic of graphite. However, defects, impurities, and irregular bonding in amorphous carbon often hinder this transformation, creating a high-energy barrier that prevents efficient graphitisation. Hydrogen facilitates removing defective carbon bonds during shock processing or high-temperature conditions (Wang et al. 1995). It preferentially reacts with dangling bonds and carbon radicals, leading to the stabilisation of graphitic layers. Due to its high thermal conductivity, the presence of hydrogen in the driven gas mixture can make it a better quencher than inert Ar

ORIGINAL UNEDITED MANUSCRIPT

Downloaded from academic.oup.com/mnras/advance-article/doi/10.1093/mnras/stag2104/9013336 by The Templeman Library user on 06 November 2026

(Wang et al. 1995). To investigate the role of hydrogen in shock-induced graphitization, Roy *et al.* (2026) recently performed a separate set of shock-tube experiments on amorphous carbon nanopowder in the presence of hydrogen. In these experiments, approximately 0.1 g of amorphous carbon nanopowder was shock processed at a reflected shock temperature of ~3900 K under a hydrogen-containing atmosphere, simulating low-velocity interstellar shock conditions. The recovered samples were characterized using Raman spectroscopy and high-resolution transmission electron microscopy (HRTEM). The results reveal enhanced graphitization together with the formation of several carbon nanostructures, including carbon nanotubes, carbon nano-onions, and nanodiamonds Roy *et al.* (2026).

Interestingly, these nanostructures are similar to those reported in our previous study (Roy et al. 2022b), where comparable carbon nanostructures were produced by shock processing amorphous carbon at a much higher reflected shock temperature (~7300 K) in the absence of hydrogen. The observation of similar structural transformations at a substantially lower temperature in the presence of hydrogen suggests that atomic hydrogen promotes graphitization and facilitates the structural reorganization of amorphous carbon under shock conditions.

5. Astrophysical Implications:

C-rich AGB stars show a strong infrared excess, which can be attributed to the combined presence of amorphous carbon and SiC (Groenewegen 1995). The gas in the inner region of AGB stars comprises H_2, H, He, CO, C_2H_2, CH_4, and organosilicon molecules such as SiH_4, SiC_2, Si_2C, SiC_3, SiC_4, SiCN, SiH_3CN, CH_3SiH_3 etc. ((Accolla et al. 2021), and reference therein). Pulsations from AGB stars can create shock waves which propagate away from their photospheres and subsequently alter the layer of the gas in the propagating medium (Bowen 1988, Cherchneff *et al.* 1992). These pulsation-created shock waves usually have a velocity of around < 20 km s^{-1} and do not have sufficient energy to ionise the atoms and molecules present in the medium. However, these low-velocity shocks can thermalize the gas and dust in its path (Fox & Wood 1985). This in turn can produce thermally and electronically excited C and Si atoms from the amorphous carbon, hydrocarbon molecules and organosilicon molecules. These excited atoms can react with the hydrocarbon molecules or radicals via equations (9-10), as suggested by (MacKay & Charnley 1999) leading to the formation of Si-C bonds, which serve as a basic building

ORIGINAL UNEDITED MANUSCRIPT

Downloaded from academic.oup.com/mnras/advance-article/doi/10.1093/mnras/stag2104/9013336 by The Templeman Library user on 06 November 2026

block of the SiC dust. The present work shows that in extreme shock conditions, ~ 5.3 M and reflected shock temperatures of ~ 3900 K, C and Si can react to make bi-phase SiC dust along with various other carbon nanostructures such as carbon nanoribbons, MWCNT, nanobuds, and graphite in the presence of hydrogen. Our results suggest that the presence of low-velocity shocks within the envelopes of carbon-rich AGB stars can trigger the simultaneous formation of SiC and various types of carbon allotropes.

In the planetary nebula Tc1, fullerene has been reported along with the SiC (Cami *et al.* 2010). Different pathways have been explored to address the formation of fullerene in this planetary nebula. To date, two different formation pathways have been proposed to synthesise carbonaceous dust grains in the ISM. The bottom-up formation route deals with the formation of dust grains from the atomistic scale. The top-down formation pathway shows that smaller dust grains can be synthesised by breaking the pre-existing larger grains through energetic processing (Cami *et al.* 2018, Roy et al. 2022b, Roy et al. 2023). Bernal et al (Bernal et al. 2019, Bernal et al. 2022) have shown a top-down formation route to fullerene formation by heavy ion irradiation of the SiC grains. Based on the results of photo - processing of HAC grains by Scott et al 1996. Garcia Harnandez et al, 2010 proposed a top-down formation of a route to fullerene in Tc-1 from HAC. Roy et al (Roy et al. 2022b) showed a shock-induced bottom-up formation route, leading to the formation of multi-shell fullerene and other carbon nanostructures from amorphous carbon in a hydrogen-free environment. In this work, we have shown that the fullerene and SiC observed in the Tc-1 can be formed simultaneously by shocking the amorphous carbon and Si nano dust mixtures in the presence of hydrogen. In addition, our results also suggest that the presence of bi-phase SiC in meteorites could be the product of shock processed dust before accretion.

The outcomes of this work applies to the regions where low velocity shocks are present in the interstellar medium. Shock waves in the interstellar space give rise different events while interacting with the matter present in its propagation medium. The high velocity shock waves with velocity more than 100 km s^{-1} destroy the grains by events such as sputtering, shattering and grain charging (Jones et al. 1996). Whereas, the low velocity shock wave with velocity < 10 km/s dominates over the thermal processing and leading to physico chemical changes of dust grains (Rudnitskij 1997). Also in the interstellar

ORIGINAL UNEDITED MANUSCRIPT

Downloaded from academic.oup.com/mnras/advance-article/doi/10.1093/mnras/stag2104/9013336 by The Templeman Library user on 06 November 2026

space, the shock processing is not an isolated event, it has always been accompanied by ion and UV, X ray processing, which further influence dust evolution (Arumainayagam et al. 2019).

The shock tube often mimics these low-velocity interstellar shocks in controlled laboratory conditions (Biennier et al. 2017, Roy et al. 2022b, Roy et al. 2022a, Roy et al. 2025). The primary focus of shock tube studies is to probe the effects of shock-induced flash heating on the physico-chemical properties of astrophysical dust analogues. Although the pressure generated during reflected shock heating is much higher than that of the ISM or CSM, the excess pressure in the shock tube is unavoidable and produces transient high temperatures (~3900 K in this work) for millisecond order times. Therefore, shock tube experiments are intended to reproduce the thermal history associated with shock-induced flash heating of dust grains that mimics a part of the conditions experienced in the ISM or CSM.

Shock tube experiments can provide unique extreme conditions in terms of heating and cooling but its heating time is limited to 2 ms only, which is less compared to the interstellar shocks where the shock processing happened over a thousands of years, depending on the phase of ISM (Jones et al. 1996). In addition to that shock tube experiments do not simultaneously study the combined effect of UV photons, X-rays, cosmic rays, magnetic fields, and the extremely low gas densities of CSM and the ISM. Therefore, the present results should be considered as providing insight into the fundamental mechanisms of shock-induced dust processing in a simulated low velocity (~ 1.8 km s^{-1}) regime which is a part of the astrophysical conditions.

6. Conclusions:

We have studied the fate of a mixture of amorphous carbon (particle size < 100 nm) and Si nanopowder subjected to extreme shock conditions (5.1 M, 3900 K) in the presence of molecular hydrogen. The analysis of the shocked sample showed the presence of SiC, in both cubic (β) and hexagonal phase, with the dominance of β-SiC. We also observed the presence of various carbon nanostructures such as carbon nanoribbons, MWCNT, nanobuds, and graphite. The results from these experiment suggest that SiC and other graphitic carbon nanostructures could be an abundant and early high-temperature condensate product that are formed simultaneously in the low-velocity shock-processed region of C-rich AGB stars. In the future, we will explore the formation route of other astrophysically relevant

ORIGINAL UNEDITED MANUSCRIPT

Downloaded from academic.oup.com/mnras/advance-article/doi/10.1093/mnras/stag2104/9013336 by The Templeman Library user on 06 November 2026

organosilicon molecules via shock processing.

Data Availability: The complete set of data will be made available on reasonable request to the corresponding author(s).

Acknowledgement:
AR, SVS, RR, JKM, KKM, JP, AB and BS acknowledge Physical Research Laboratory (Ahmedabad), Department of Space - Govt of India for their support. AR, SVS, RR, JKM and BS acknowledge the Centre for Nanoscience and Engineering (CeNSE), IISc, Bengaluru, India for the HR-TEM facility. The authors acknowledge the Central Instrumental Facility of IIT–Gandhinagar. AR, RR, JKM, NJM and BS acknowledges the support from Sir John and Lady Mason academic trust.

AR acknowledge his Senior Research Fellowship and Postdoctoral Fellowship in Physical Research Laboratory, Ahmedabad, India. JP acknowledges the support of an INSA Senior Scientist Fellowship. NJM acknowledges support of Europlanet 2024 RI from the European Union's Horizon 2020 research and innovation programme under grant agreement No 871149 and Royal Society awards IEC\R3\223083 and IES\R3\223221during the course of this work.

References:

Abràmoff M.D., Magalhães P.J., Ram S.J., 2004, Biophotonics international, 11, 36
Accolla M., et al., 2021, The Astrophysical Journal, 906, 44
Amari S., 2014, Mass Spectrometry, 3, S0042
Apponi A., McCarthy M., Gottlieb C., Thaddeus P., 1999, The Astrophysical Journal, 516, L103
Arumainayagam C.R., et al., 2019, Chemical Society Reviews, 48, 2293
Bernal J., Haenecour P., Howe J., Zega T., Amari S., Ziurys L., 2019, The Astrophysical Journal Letters, 883, L43
Bernal J.J., Zega T.J., Ziurys L.M., 2022, The Journal of Physical Chemistry A, 126, 5761
Bernatowicz T., Fraundorf G., Ming T., Anders E., Wopenka B., Zinner E., Fraundorf P., 1987, Nature, 330, 728
Biennier L., et al., 2017, Astronomy & Astrophysics, 599, A42
Bowen G., 1988, The Astrophysical Journal, 329, 299
Bundy F., 1964, The Journal of Chemical Physics, 41, 3809
Bundy F., 1989, Physica A: Statistical Mechanics and its Applications, 156, 169
Cami J., Bernard-Salas J., Peeters E., Malek S.E., 2010, Science, 329, 1180
Cami J., Peeters E., Bernard-Salas J., Doppmann G., De Buizer J., 2018, Galaxies, 6, 101
Carmer C.S., Frenklach M., 1989, Applied physics letters, 54, 1430
Cernicharo J., Gottlieb C., Guelin M., Thaddeus P., Vrtilek J., 1989, The Astrophysical Journal, 341, L25
Cernicharo J., et al., 2015, The Astrophysical Journal Letters, 806, L3
Cernicharo J., et al., 2010, Astronomy and Astrophysics, 521, L8

ORIGINAL UNEDITED MANUSCRIPT

Downloaded from academic.oup.com/mnras/advance-article/doi/10.1093/mnras/stag2104/9013336 by The Templeman Library user on 06 November 2026

Chakraborty S., et al., 2024, Astronomy & Astrophysics, 681, A39
Chen T., Xiao C., Li A., Zhou C., 2022, Monthly Notices of the Royal Astronomical Society, 509, 5231
Cherchneff I., 2000, Symposium-International Astronomical Union. Cambridge University Press, p. 331
Cherchneff I., Barker J.R., Tielens A.G., 1992, The Astrophysical Journal, 401, 269
Daulton T.L., Bernatowicz T.J., Lewis R.S., Messenger S., Stadermann F.J., Amari S., 2003, Geochimica et Cosmochimica Acta, 67, 4743
Derjaguin B., Fedoseev D., Varnin V., Vnukov S., 1977, Nature, 269, 398
Dhage R., Roy A., Sivaraman B., Rajyaguru P.I., 2025, PNAS nexus, 4, pgaf300
Ellerbrock R., Stein M., Schaller J., 2022, Scientific Reports, 12, 11708
Fox M., Wood P., 1985, Astrophysical Journal, Part 1 (ISSN 0004-637X), vol. 297, Oct. 15, 1985, p. 455-475., 297, 455
Frenklach M., Carmer C., Feigelson E., 1989, Nature, 339, 196
Friedemann C., 1969, Physica, 41, 139
Gilman R.C., 1969, Astrophysical Journal, vol. 155, p. L185, 155, L185
Goebel J., et al., 1980, Astrophysical Journal, Part 1, vol. 235, Jan. 1, 1980, p. 104-113., 235, 104
Groenewegen M., 1995, Astronomy and Astrophysics, Vol. 293, p. 463-478 (1995), 293, 463
Gyngard F., Zinner E., Nittler L.R., Morgand A., Stadermann F.J., Hynes K.M., 2010, The Astrophysical Journal, 717, 107
Hackwell J., 1972, Astronomy and Astrophysics, 21, 239
Heck P.R., et al., 2009, The Astrophysical Journal, 698, 1155
Heine V., Cheng C., Needs R.J., 1991, Journal of the American Ceramic Society, 74, 2630
Hofmeister A.M., Pitman K., Goncharov A., Speck A.K., 2009, The Astrophysical Journal, 696, 1502
Hoppe P., Leitner J., Gröner E., Marhas K.K., Meyer B.S., Amari S., 2010, The Astrophysical Journal, 719, 1370
Huisken F., Kohn B., Alexandrescu R., Cojocaru S., Crunteanu A., Ledoux G., Reynaud C., 1999, Journal of Nanoparticle Research, 1, 293
Izumi F., Momma K., 2007, Solid State Phenomena, 130, 15
Jones A., Tielens A., Hollenbach D., 1996, The Astrophysical Journal, 469, 740
Jones A., Ysard N., 2022, Astronomy & Astrophysics, 657, A128
Kakimoto K., Nakano S., 2025, Journal of Crystal Growth, 128332
Knippenberg W.F., 1963, Philips Research Report, 18, 161
Kumar V., et al., 2022, Monthly Notices of the Royal Astronomical Society, 510, 4265
Kusunoki M., Rokkaku M., Suzuki T., 1997, Applied Physics Letters, 71, 2620
Langenderfer M.J., Zhou Y., Watts J., Fahrenholtz W.G., Johnson C.E., 2022, Ceramics International, 48, 4456
Li Z., Lu C., Xia Z., Zhou Y., Luo Z., 2007, Carbon, 45, 1686
Loh G., Baillargeat D., 2013, Journal of applied physics, 114
MacKay D., Charnley S., 1999, Monthly Notices of the Royal Astronomical Society, 302, 793
Martínez L., et al., 2020, Nature Astronomy, 4, 97
McCabe E., 1982, Monthly Notices of the Royal Astronomical Society, 200, 71
Merino P., et al., 2014, Nature Communications, 5, 1
Mutschke H., Andersen A.C., Clément D., Henning T., Peiter G., 1999, arXiv preprint astro-ph/9903031,
Ohishi M., et al., 1989, Astrophysical Journal, Part 2-Letters (ISSN 0004-637X), vol. 345, Oct. 15, 1989, p. L83-L86. Research supported by the Morino Science Foundation., 345, L83
Ott U., 2010, Astromineralogy. Springer, p. 277
Patch R.W., 1962, The Journal of Chemical Physics, 36, 1919
Pitts W.M., Pasternack L., McDonald J., 1982, Chemical Physics, 68, 417
Roy A., et al., 2022a, Monthly Notices of the Royal Astronomical Society, 517, 4845
Roy A., et al., 2025, RSC advances, 15, 12309
Roy A., et al., 2026, EPJ Web of Conferences. EDP Sciences, p. 03001
Roy A., et al., 2022b, Advances in Space Research,

ORIGINAL UNEDITED MANUSCRIPT

Downloaded from academic.oup.com/mnras/advance-article/doi/10.1093/mnras/stag2104/9013336 by The Templeman Library user on 06 November 2026

Roy A., et al., 2023, Journal of the Indian Institute of Science**,** 1
Rudnitskij G., 1997, Astrophysics and Space Science*,* 251**,** 259
Santoro G., et al., 2020, The Astrophysical Journal*,* 895**,** 97
Scalise E., Marzegalli A., Montalenti F., Miglio L., 2019, Physical Review Applied*,* 12**,** 021002
Sevenster M.N., Chapman J.M., 2001, The Astrophysical Journal*,* 546**,** L119
Singh D.K., et al., 2025, Astronomy & Astrophysics*,* 704**,** A345
Singh S.V., et al., 2020, Molecules*,* 25**,** 5634
Sorrell W.H., 1990, Monthly Notices of the Royal Astronomical Society (ISSN 0035-8711), vol. 243, April 15, 1990, p. 570-587.*,* 243**,** 570
Speck A., Barlow M., Skinner C., 1997, Monthly Notices of the Royal Astronomical Society*,* 288**,** 431
Speck A.K., Corman A.B., Wakeman K., Wheeler C.H., Thompson G., 2009, The Astrophysical Journal*,* 691**,** 1202
Spitzer W., Kleinman D., Walsh D., 1959, Physical Review*,* 113**,** 127
Thaddeus P., Cummins S., Linke R., 1984, Astrophysical Journal, Part 2-Letters to the Editor (ISSN 0004-637X), vol. 283, Aug. 15, 1984, p. L45-L48.*,* 283**,** L45
Treffers R., Cohen M., 1974, Astrophysical Journal, Vol. 188, p. 545-552*,* 188**,** 545
Van de Steene G., Van Hoof P., 2003, Astronomy & Astrophysics*,* 406**,** 773
Wang X., Lin X., Mesleh M., Jarrold M., Dravid V., Ketterson J., Chang R., 1995, Journal of Materials Research*,* 10**,** 1977
Watanabe H., Hisada Y., Mukainakano S., Tanaka N., 2001, Journal of microscopy*,* 203**,** 40
Whittet D., Duley W., Martin P., 1990, Monthly Notices of the Royal Astronomical Society (ISSN 0035-8711), vol. 244, June 1, 1990, p. 427-431. Research supported by SERC and NSERC.*,* 244**,** 427
Willhardt C., Chen D., Daniel K., Guildenbecher D., Glumac N., 2024, Combustion and Flame*,* 265**,** 113468

ORIGINAL UNEDITED MANUSCRIPT

Downloaded from academic.oup.com/mnras/advance-article/doi/10.1093/mnras/stag2104/9013336 by The Templeman Library user on 06 November 2026